Red (Eu^{3+}), Green (Tb^{3+}) and Ultraviolet (Gd^{3+}) Emitting Nitrilotriacetate Complexes Prepared by One-step Synthesis

Ivan G. N. Silva[a], Hermi F. Brito[a], Ernesto R. Souza[a], Danilo Mustafa[a], Maria C. F. C. Felinto[b], Luis D. Carlos[c], and Oscar L. Malta[d]

[a] Departamento de Química Fundamental, Instituto de Química da Universidade de São Paulo, 05508-900, São Paulo, SP, Brazil
[b] Instituto de Pesquisas Energéticas e Nucleares, IPEN, Cidade Universitária, 05508-000, São Paulo, SP, Brazil
[c] Department of Physics, CICECO, University of Aveiro, Campus, Universitário de Santiago, 3810–193, Aveiro, Portugal
[d] Departamento de Química Fundamental, CCEN, Universidade Federal da Pernambuco, 50670-901, Recife, PE, Brazil

Reprint requests to H. F. Brito. Phone: +55-11-3091-3708. E-mail: hefbrito@iq.usp.br

Z. Naturforsch. **2014**, *69b*, 231 – 238 / DOI: 10.5560/ZNB.2014-3263
Received September 11, 2013

The $[RE(NTA)(H_2O)_2]\cdot(H_2O)$ rare-earth complexes (RE^{3+}: Eu, Gd, Tb and NTA: nitrilotriacetate) were synthesized and characterized by elemental analysis, thermogravimetry, X-ray diffraction, and infrared spectroscopy. The complexes show high crystallinity and thermostability. The photoluminescence behavior was studied based on the excitation and emission spectra, and luminescence decay curves. The compounds exhibit red (Eu^{3+}), green (Tb^{3+}) and UV (Gd^{3+}) monochromatic emissions under UV excitation. The NTA ligand acts as luminescence sensitizer in the ligand-to-RE^{3+} intramolecular energy transfer process, owing to the fact that the first excited triplet state (T_1: 29 000 cm^{-1}) is located above of the $^5D_0$ (Eu^{3+}) and $^5D_4$ (Tb^{3+}) emitting levels. The experimental intensity parameters Ω_λ (λ: 2 and 4) for the Eu^{3+} NTA complex were calculated, and the results are discussed. The Gd^{3+}-NTA complex exhibits a high-intensity emission band in the UV region (32 000 cm^{-1}) assigned to the $^6P_{7/2} \rightarrow {}^8S_{7/2}$ intraconfigurational transition.

Key words: Rare-Earth Complexes, Tricarboxylates, Synthesis, Intramolecular Energy Transfer, Photoluminescence

Introduction

Complexes containing carboxylate ligands have been studied in many research areas due to the variety of their molecular structures which enables different chemical applications such as gas storage systems [1] or nanostructured magnetic materials [2]. These properties allow the construction of a wide range of materials and their widespread use in many areas, such as the synthesis of precursor materials [3], immunoassays [4] and optical markers [5]. The rare-earth complexes (*RE*) have been widely used as organic light-emitting devices (OLEDs) [6], emergency signage [7], luminescence markers [8], display panels [9], among others.

The spectroscopic properties of the *RE* elements are based on their peculiar electronic configuration of the filled $5s^2$ and $5p^6$ subshells which are beyond the $4f$ subshell, shielding it efficiently from the chemical environment and providing monochromatic emission [10]. Therefore, the RE^{3+} ions present narrow absorption and emission bands, maintaining their atomic character, which facilitates the interpretation of their energy level structures [11].

The RE^{3+} ions have low molar absorption coefficients because the $4f$ intraconfigurational transitions are forbidden by the Laporte rule, so the probability of these transitions is very low. In order to overcome this shortcoming, coordinating ligands such as carboxylate and β-diketonate groups are widely used, mainly be-

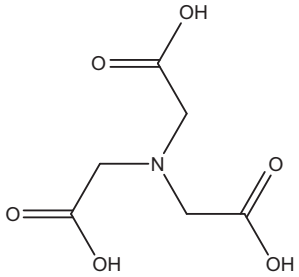

Fig. 1. Structural formula of nitrilotriacetic acid, H_3(NTA).

cause of their high absorptivity coefficient in the UV region and the luminescence-sensitizing abilities [12]. This phenomenon is often denoted as the *antenna effect*, largely used in the design of luminescent RE^{3+} complexes [13].

Nitrilotriacetic acid H_3(NTA), depicted in Fig. 1 is applied mostly in aqueous solution since the NTA ligand can be used as a biodegradable and biologically compatible substitute for EDTA as carrier of a large variety of metal ions [14, 15]. There are studies about the optical behavior of the RE^{3+} nitrilotriacetate complexes in solution [16, 17].

In this article, we report the one-step synthesis of complexes of the type $[RE(NTA)(H_2O)_2]\cdot(H_2O)$ and the study of their luminescence properties in the solid state. Photoluminescence data were obtained from the excitation, emission spectra and luminescence decay curves. The energy transfer processes from NTA excited states to the intraconfigurational states of the RE^{3+} ions were also investigated. The experimental intensity parameters (Ω_2 and Ω_4) were determined using the $^5D_0 \rightarrow {}^7F_{2,4}$ transitions.

Experimental Section

Nitrilotriacetic acid (97 %, Sigma-Aldrich) was used without further purification. The NTA^{3-} ligand solution was prepared by adding NaOH (1.0 M) to the aqueous ligand suspension until pH ≈ 6. The rare-earth chlorides $RECl_3\cdot(H_2O)_6$ were obtained from their oxides (99.99 %) Eu_2O_3 and Gd_2O_3 by dissolution in concentrated HCl, Tb_4O_7 was treated with addition of H_2O_2. The obtained crystalline solids were dried on a water bath and stored under reduced pressure.

Syntheses

The RE^{3+}-NTA complexes were prepared by adding 50 mL of the $RECl_{3(aq)}$ solution (0.050 M) dropwise to 200 mL of the NTA^{3-} ligand solution (0.0125 M) and heating the mixture at the boiling point for 4 h. The precipitates were filtered and washed three times with distilled water [18]. The rare-earth complexes are colorless crystalline powders, non-hygroscopic and insoluble in acetone, ethanol, DMSO, acetonitrile and chloroform.

$[Eu(NTA)(H_2O)_2]\cdot(H_2O)$: Elemental analysis (%) for $C_6H_{12}NO_9Eu$: calcd. C 18.28, H 3.07, N 3.5, Eu 38.56; found C 18.41, H 2.92, N 3.55, Eu 39.02. *$[Gd(NTA)(H_2O)_2]\cdot(H_2O)$*: Elemental analysis (%) for $C_6H_{12}NO_9Gd$: calcd. C 18.04, H 3.03, N 3.51, Gd 39.37; found C 18.14, H 2.92, N 3.41, Gd 39.74. *$[Tb(NTA)(H_2O)_2]\cdot(H_2O)$*: Elemental analysis (%) for $C_6H_{12}NO_9Tb$: calcd. C 17.97, H 3.02, N 3.49, Tb 39.62; found C 18.11, H 2.96, N 3.45, Tb 39.80.

Elemental analyses were performed with a Perkin-Elmer CHN 2400 analyzer. The complexometric titrations were performed using a microburette with the disodium ethylenediaminetetraacetic acid (EDTA) salt. The XRD patterns were recorded on a Miniflex Rigaku instrument (CuK_{α_1}) from 4 to 60° (2θ). The infrared absorption spectra (FTIR) were performed using KBr pellets with a Bomem MB100 FTIR instrument in the spectral region from 400 to 4000 cm^{-1}. Thermogravimetry curves were obtained with the TA Instruments HI-RES TGA 2850 equipment from 30 to 900 °C in a dynamic atmosphere of synthetic air with a constant heating ramp of 5 °C min^{-1}.

The luminescence study was based on the excitation and emission spectra recorded at room temperature (300 K) and in liquid nitrogen (77 K). The data were collected in front face mode (22.5°) with a 450 W xenon lamp as excitation source coupled to a SPEX-Fluorolog 2 instrument with double monochromators. Luminescence decay curves were recorded using a SPEX 1934D phosphorimeter accessory with a 150 W pulsed lamp.

Results and Discussion

Characterization

The elemental analyses and complexometric titrations confirmed the molar ratio of *RE* to NTA (1 : 1) and three water molecules, resulting in the general formula $[RE(NTA)(H_2O)_2]\cdot(H_2O)$ where RE^{3+}: Eu, Gd and Tb.

XRD patterns of the Eu^{3+}, Gd^{3+} and Tb^{3+} complexes and the calculated data based on the $[Sm(NTA)(H_2O)_2]\cdot(H_2O)$ structure obtained by Yu *et al.* [19] are presented in Fig. 2. The experimental and calculated XRD patterns are very similar, suggesting an isomorphic complex series. The coordination geometry of the RE^{3+} center can be described as a capped

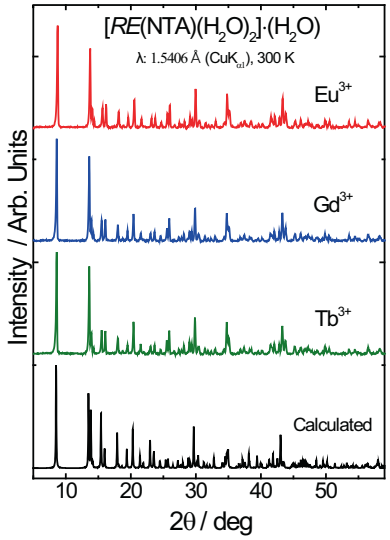

Fig. 2 (color online). Powder X-ray diffraction patterns of $[RE(NTA)(H_2O)_2]\cdot(H_2O)$ complexes (RE^{3+}: Eu, Gd and Tb) recorded at room temperature, and calculated data.

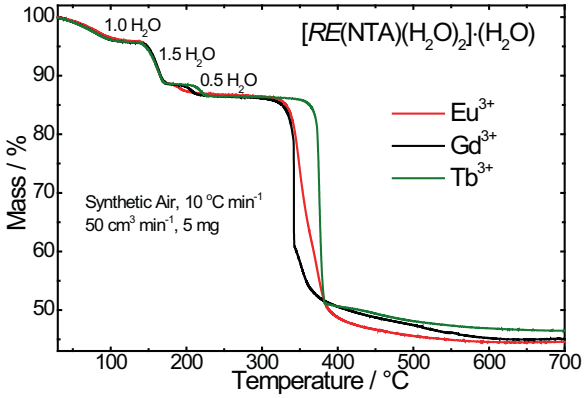

Fig. 3 (color online). Thermogravimetric curves of $[RE(NTA)\cdot(H_2O)_2]\cdot(H_2O)$ solid samples (RE^{3+}: Eu, Gd and Tb). All curves were recorded in dynamic synthetic air atmosphere.

square antiprism. The coordination occurs by the carboxylate oxygen atoms (monodentate and bridging), the nitrogen atom of the NTA ligand and two water molecules [19].

The FTIR absorption spectra of the RE^{3+} complexes show the characteristic symmetric (ν_s) and asymmetric (ν_{as}) stretching of the carboxylate group around 1690 and 1405 cm^{-1}, respectively. The difference between these values ($\Delta\nu$) is similar for all the complexes (285 cm^{-1}), and the $\Delta\nu$ of the sodium salt (Na_3NTA) is around 340 cm^{-1} (1730 and 1390 cm^{-1}), indicating monodentate and bridging coordination through the oxygen atoms [20]. Moreover, the spectra exhibit a broad band in the spectral range from 3000 to 3600 cm^{-1} assigned to the O–H stretching vibration of water molecules. The spectra also show a sharp peak around 3560 cm^{-1} which is assigned to free O–H stretching vibration of H_2O molecule coordinated to the RE^{3+} ions, indicating that these water molecules do not take part in hydrogen bonding [21].

The thermogravimetric analyses of the RE^{3+}-NTA complexes (Fig. 3) show three events assigned to the loss of water molecule in the temperature interval from 30 to 250 °C. The first and the second events occur from 30 to 140 °C and from 140 to 175 °C and correspond to the loss of 1 and 1.5 water molecule, respectively. The last event corresponds to the loss of 0.5 water molecule between 175 °C and a final at 205 (Eu^{3+}), 215 (Gd^{3+}) and 225 °C (Tb^{3+}) (Fig. 3) possibly associated with the decrease of rare-earth ionic radii of 94.7, 93.8 and 92.3 pm, respectively. The TG data agree with the elemental analysis and IR data, which show vibrational stretching modes indicative of more than one type of water molecules in the RE^{3+} complexes. The thermal decomposition of the ligands in the complexes occurs between 320 and 600 °C. No events are observed after a calcination temperature at around 600 °C, suggesting the formation of Eu_2O_3 and Gd_2O_3 (colorless) or Tb_4O_7 (brown).

Photoluminescence study

The Gd^{3+}-NTA complex

Gadolinium complexes have been used to determine the first triplet state (T_1) of ligands [22], since there is a large energy gap ($\sim$ 32 000 cm^{-1}) between the $^8S_{7/2}$ ground state and the first $^6P_{7/2}$ excited state of the Gd^{3+} ion. Normally, this energy cannot be afforded from the lower-laying first excited T_1 state of the organic ligands *via* intramolecular energy transfer from ligand-to-Gd^{3+} ion. The ligand T_1 state energy is taken from the highest emission energy in the triplet state in the gadolinium complexes, which corresponds to the zero phonon transition [22].

The excitation spectrum at 77 K with emission monitored at 435 nm shows a broad band from 250 to

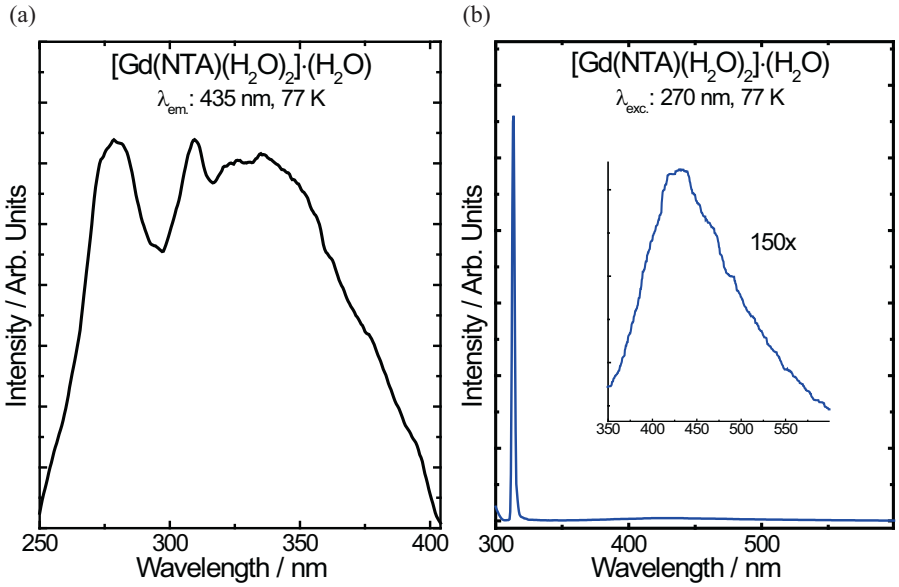

Fig. 4 (color online). The excitation spectrum of $[Gd(NTA)(H_2O)_2]\cdot(H_2O)$ (a), with emission monitored at 435 nm, and the emission spectrum (b), with excitation at 270 nm, recorded at 77 K.

400 nm that is assigned to the $S_0 \rightarrow S_n$ singlet states of the NTA ligand (Fig. 4a).

The emission spectrum of the $[Gd(NTA)(H_2O)_2]\cdot(H_2O)$ complex recorded at 77 K, under excitation at 270 nm (inset Fig. 4b), indicates that the T_1 state zero phonon transition of the ligand is around 29 000 cm^{-1}. The high energy of the triplet state in the NTA ligand can be explained by the absence of conjugation of π bonds [9, 23]. The T_1 state energy of the NTA ligand is higher than the $^5D_0$ ($\sim$ 17 290 cm^{-1}) and $^5D_4$ ($\sim$ 20 400 cm^{-1}) emitting levels of Eu^{3+} and Tb^{3+} ions, respectively. However, it is located below the $^6P_{7/2}$ ($\sim$ 32 000 cm^{-1}) emitting level of the Gd^{3+} ion. This spectroscopic behavior demonstrates that the NTA ligand can act as a luminescence sensitizer in the intramolecular energy transfer process for the Eu^{3+} and Tb^{3+} complexes.

It is noteworthy that the emission spectrum of the $[Gd(NTA)(H_2O)_2]\cdot(H_2O)$ complex shows an exceptional narrow emission band arising from the $^6P_{7/2} \rightarrow {}^8S_{7/2}$ transition of the gadolinium ion. This result suggests the impossibility of intramolecular energy transfer from the NTA ligand singlet states to the $^6P_{7/2}$ excited state of Gd^{3+}, located at lower energy than the S_1 excited state of the ligand. Therefore, this complex can be used as luminescence probe in the UV region due to the presence of a high-intensity monochromatic emission at 31 950 cm^{-1} (Fig. 4).

The Tb^{3+}-NTA complex

The green emission of Tb^{3+}-containing compounds around 546 nm under UV excitation is due to the high emission intensity of the $^5D_4 \rightarrow {}^7F_5$ transition [24]. Intramolecular energy transfer can be interpreted in terms of energy transfer from the lowest triplet state of the NTA ligand (T_1) to the $^5D_4$ state or higher excited states composed mainly of the $^5L_8$, $^5G_3$, $^5G_4$, and $^5D_2$ levels. The energy transfer occurs more efficiently when the energy gap is higher than 2000 cm^{-1}, avoiding the back energy transfer [25 – 28].

Fig. 5a shows the excitation spectrum of the $[Tb(NTA)(H_2O)_2]\cdot(H_2O)$ complex with emission monitored at 545 nm and the emission spectrum with excitation at 300 nm at 77 K. The broad absorption bands of the NTA ligand are overlapping with the principal narrow bands originating from the $^7F_6$ ground state to the ^5D_J, ^5F_J, ^5G_J, ^5H_J, ^5K_J, and ^5L_J excited states of the Tb^{3+} ion.

The emission spectrum of the Tb^{3+} complex (Fig. 5b) presents sharp peaks assigned to the $^5D_4 \rightarrow {}^7F_J$ transitions of the Tb^{3+} ion (J: 6–0): $^7F_6$

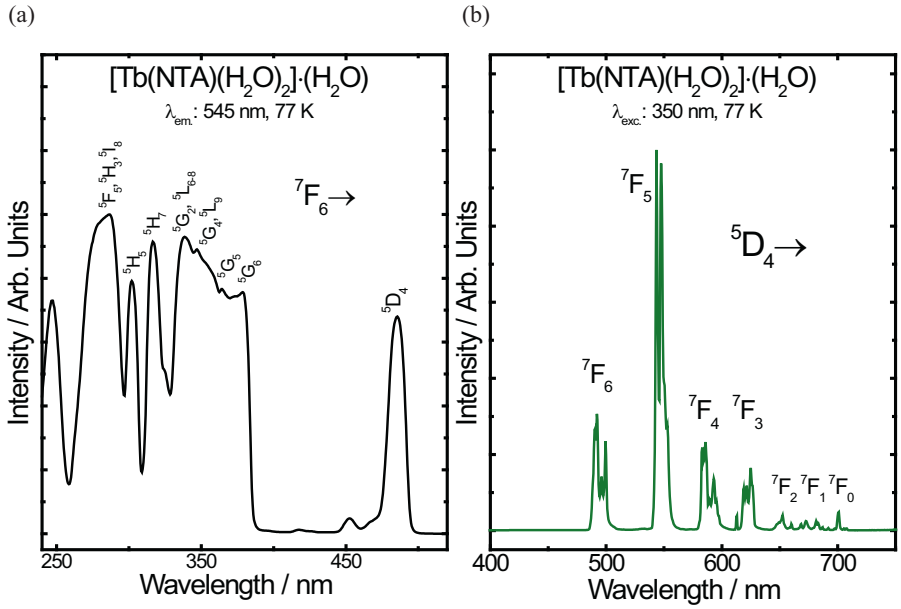

Fig. 5 (color online). The excitation spectrum of $[Tb(NTA)(H_2O)_2]\cdot(H_2O)$ (a), with emission monitored at 545 nm, and the emission spectrum (b), with excitation at 350 nm, recorded at 77 K.

(20 283); $^7F_5$ (18 281); $^7F_4$, (17 094); $^7F_3$ (16 051); $^7F_2$ (15 360); $^7F_1$ (14 749) and $^7F_0$ (14 285 cm^{-1}). The efficient energy transfer from the NTA ligand to the Tb^{3+} ion is confirmed by the absence of any broad emission band.

The Eu^{3+}-NTA complex

The excitation spectrum of $[Eu(NTA)\cdot(H_2O)_2]\cdot(H_2O)$ was recorded at 77 K and monitored at 613 nm (Fig. 6a). The absorption bands originate from the $^7F_0$ ground state to the excited levels ^5L_J: $^5D_0$ (17 276); $^5D_1$ (19 065); $^5D_2$ (21 538); $^5D_3$ (24 454); $^5L_6$ (25 379); $^5L_7$ (26 737); $^5D_4$ (27 751); $^5H_3$ (31 538), $^5F_2$ (33 626); $^5F_4$ (35 144 cm^{-1}) (Fig. 6a). The $^7F_0 \rightarrow {}^5L_6$ transition (25 379 cm^{-1}) exhibits the highest absorption intensity among the $4f^6$ intraconfigurational transitions, indicating that this transition is more efficient for the direct excitation of the Eu^{3+} ion. The absence of the NTA absorption bands in Fig. 6a is due to the large energy gap between the T_1 and $^5D_0$ states, suggesting that the energy transfer ligand-Eu^{3+} is not as efficient as in the Tb^{3+} compound.

Fig. 6b shows the narrow emission bands originating from the $^5D_0$ emitting level of Eu^{3+}: $^7F_0$ (17 276); $^7F_1$ (16 835); $^7F_2$, (16 181); $^7F_3$ (15 290); $^7F_4$ (14 367); $^7F_5$ (13 440 cm^{-1}) and from the $^5D_1$ emission level: $^7F_0$ (18 975); $^7F_1$ (18 587) and $^7F_2$ (17 953 cm^{-1}). According to the $(2J+1)$-manifold, the $^5D_0 \rightarrow {}^7F_J$ splitting suggests that the Eu^{3+} ion has a low-symmetry environment. It is worth to mention that the $^5D_0 \rightarrow {}^7F_0$ shows only one peak which indicates that the metal ions have only one symmetry site.

The radiative rates ($A_{0\rightarrow J}$) for $^5D_0 \rightarrow {}^7F_2$ were calculated using Eq. 1 [29, 30],

$$A_{0\rightarrow J} = \frac{\sigma_{0\rightarrow 1}}{S_{0\rightarrow 1}} \frac{S_{0\rightarrow J}}{\sigma_{0\rightarrow J}} A_{0\rightarrow 1} \qquad (1)$$

where $\sigma_{0\rightarrow 1}$ and $\sigma_{0\rightarrow J}$ correspond to the energy barycenters of the $^5D_0 \rightarrow {}^7F_1$ and $^5D_0 \rightarrow {}^7F_J$ transitions, respectively. $S_{0\rightarrow 1}$ and $S_{0\rightarrow J}$ are the areas of the emission curve corresponding to the $^5D_0 \rightarrow {}^7F_1$ and $^5D_0 \rightarrow {}^7F_J$ transitions, respectively [31]. Since the magnetic dipole transition $^5D_0 \rightarrow {}^7F_1$ is almost insensitive to changes in the chemical environment around the Eu^{3+} ion, the $A_{0\rightarrow 1}$ rate can be used as an internal standard to determine the $A_{0\rightarrow J}$ coefficients for Eu^{3+} complexes [30].

The lifetime (τ) of the Eu^{3+}-NTA complex was obtained from the luminescence decay curve using first order exponential decay (0.405 ms). The emission

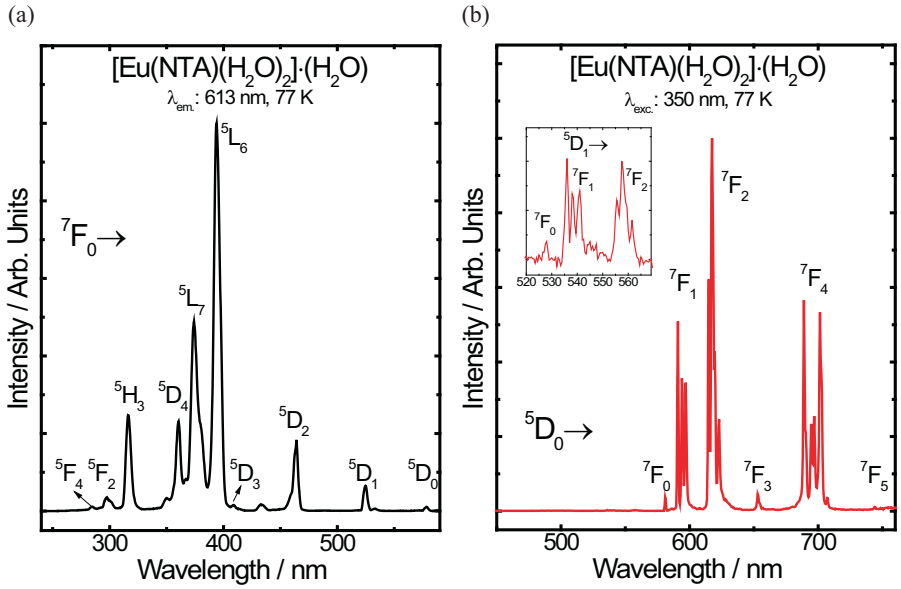

Fig. 6 (color online). The excitation spectrum of $[Eu(NTA)(H_2O)_2]\cdot(H_2O)$ (a), with emission monitored at 613 nm, and the emission spectrum (b), with excitation at 350 nm, recorded at 77 K.

quantum efficiency (η) of the $^5D_0$ emitting level is determined according to Eq. 2,

$$\eta = \frac{A_{\text{rad}}}{A_{\text{rad}} + A_{\text{nrad}}} \tag{2}$$

where the total decay rate, $A_{\text{tot}} = \frac{1}{\tau} = A_{\text{rad}} + A_{\text{nrad}}$ and $A_{\text{rad}} = \sum_J A_{0\to J}$. A_{rad} and A_{nrad} are the radiative and non-radiative rates, respectively.

The experimental intensity parameters (Ω_λ, λ: 2 and 4) are estimated from the $^5D_0 \to {}^7F_{2,4}$ transitions in the emission spectrum of the Eu^{3+} complex. The Ω_6 intensity parameter is not included in this study since the $^5D_0 \to {}^7F_6$ transition is not observed for this complex. The coefficient of spontaneous emission, A, is given by Eq. 3,

$$A = \frac{4e^2\omega^3}{3hc^3}\chi\sum_\lambda \Omega_\lambda \left\langle {}^7F_J \left\| U^{(\lambda)} \right\| {}^5D_0 \right\rangle^2 \tag{3}$$

where $\chi = \frac{n(n+2)^2}{9}$ is the Lorentz local field correction and n (1.5 for this complex) is the refraction index of the medium. The square reduced matrix elements $\langle {}^7F_J||U^{(\lambda)}||{}^5D_J\rangle^2$ are 0.0032 and 0.0023 calculated for $J = 2$ and 4, respectively [32, 33].

The values of the intensity parameters (Ω_λ) depend on the local geometry and the ligating atom polarizabilities in the first coordination sphere. The values of Ω_2 are most influenced by small angular changes in the chemical environment around the Eu^{3+} ion. The Ω_2 value of $[Eu(NTA)(H_2O)_2]\cdot(H_2O)$ is much smaller than those of $[Eu(TTA)(H_2O)_2]$ or $[Eu(BTC)(H_2O)_n]$ (BTC: EMA, TLA and TMA) (Table 1), while the ratio

Table 1. Experimental intensity parameters ($\Omega_{2,4}$), radiative (A_{rad}), non-radiative (A_{nrad}) and total (A_{tot}) rates, lifetimes of the $^5D_0$ emitting level (τ) and quantum efficiencies (η) for $[Eu(NTA)(H_2O)_2]\cdot(H_2O)$ and other representative complexes.

Eu^{3+} complexes	Ω_2 (10^{-20} cm^{-2})	Ω_4 (10^{-20} cm^{-2})	A_{rad} (s^{-1})	A_{nrad} (s^{-1})	A_{tot} (s^{-1})	τ (ms)	η (%)
$[Eu(NTA)(H_2O)_2]\cdot(H_2O)$	4	8	294	2174	2468	0.405	12
$[Eu(EMA)(H_2O)_2]$[a]	14	10	623	2015	2638	0.379	24
$[Eu(TLA)(H_2O)_4]$[a]	9	9	462	2116	2578	0.473	22
$[Eu(TMA)(H_2O)_6]$[a]	11	10	522	4345	4867	0.230	12
$[Eu(TTA)(H_2O)_2]$[b]	33	5	1110	2730	3840	0.260	29

[a] Ref. [18]; [b] ref. [22].

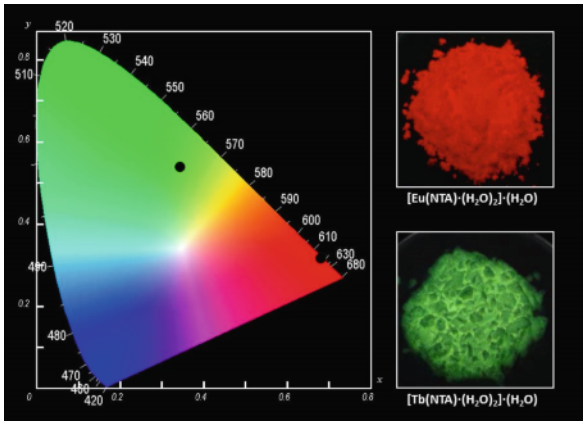

Fig. 7 (color online). CIE chromaticity diagram showing the (x, y) emission color coordinates for $[RE(\mathrm{NTA})\cdot(\mathrm{H_2O})_2]\cdot(\mathrm{H_2O})$ complexes (RE^{3+}: Eu and Tb), irradiated at 350 nm [35]. The inset figures are photographs of nanomaterials taken with a digital camera displaying the red and green emissions, respectively, under UV irradiation at 254 nm.

between Ω_4 and Ω_2 is much higher in the present compound. This spectroscopic result suggests that the coordination polyhedron has a high point symmetry like the model described in reference [34].

Table 1 presents a small emission quantum efficiency value ($\eta \sim 12\,\%$) for $[\mathrm{Eu(NTA)(H_2O)_2}]\cdot(\mathrm{H_2O})$ which can be explained owing to the presence of three water molecules in the complex.

The RE^{3+}-NTA complexes show (x, y) color coordinates in the red and green regions of the CIE chromaticity diagram (*Commission Internationale de l'Eclairage*) for Eu^{3+} (0.686, 0.309) and Tb^{3+} (0.338, 0.552) (Fig. 7). Therefore, these complexes act as light-conversion molecular devices (LCMDs) and can be applied in bicolor devices.

Conclusion

The emitting complexes $[RE(\mathrm{NTA})(\mathrm{H_2O})_2]\cdot(\mathrm{H_2O})$ were prepared in a one-step synthesis. The TG analyses show three water molecules in the structure and thermostability up to 300 °C. The XRD data indicate an isostructural series containing two coordinated and one crystal water molecules. The T_1 state of the NTA ligand has higher energy than the main $^5D_0$ (Eu^{3+}) and $^5D_4$ (Tb^{3+}) emitting levels and thus can act as intramolecular energy transfer donor to the metal ions, resulting in a red and green emission. The Tb^{3+}-NTA complex shows a more intense emission than the Eu^{3+} complex. Through excitation to higher energy states of the ligand, a monochromatic Gd^{3+} luminescence in the UV region can be obtained. The relative value of the experimental Ω_2 intensity parameter, in comparison with Ω_4, for the Eu^{3+}-NTA complex suggests a high local symmetry. Photoluminescence data show that these complexes can act as light-conversion molecular devices (LCMDs) and can be used as red, green and UV emitting luminescent materials.

Acknowledgement

We are grateful for financial support from the Conselho Nacional de Desenvolvimento Científico e Tecnológico (CNPq, Brazil), Fundação de Amparo à Pesquisa do Estado de São Paulo (FAPESP, Brazil), Instituto Nacional de Ciência e Tecnologia de Nanotecnologia para Marcadores Integrados (inct-INAMI, Brazil), Coordenação de Aperfeiçoamento de Pessoal de Nível Superior (CAPES, Brazil) and Fundação para a Ciência e a Tecnologia under contract PEst-C/CTM/LA0011/2013. L. D. C. thanks CAPES for a fellowship within the Nanobiotec network "Produção de materiais nanoparticulados para processos baseados em imunocitoquímica".

[1] U. Mueller, M. Schubert, F. Teich, H. Puetter, K. Schierle-Arndt, J. Pastre, *J. Mater. Chem.* **2006**, *16*, 626 – 636.
[2] E. J. L. McInnes, S. Piligkos, G. Timco, R. Winpenny, *Coord. Chem. Rev.* **2005**, *249*, 2577 – 2590.
[3] M. Kakihana, M. Arima, M. Yoshimura, N. Ikeda, Y. Sugitani, *J. Alloys Compd.* **1999**, *283*, 102 – 105.
[4] I. A. Hemmilä, *Application of Fluorescence in Immunoassays*, Wiley, New York, **1991**.
[5] J. Rocha, L. D. Carlos, F. A. Almeida Paz, D. Ananias, *Chem. Soc. Rev.* **2011**, *40*, 926 – 940.
[6] J. Kido, Y. Okamoto, *Chem. Rev.* **2002**, *102*, 2357 – 2368.
[7] J. Hölsä, T. Laamanen, M. Lastusaari, M. Malkamäki, P. Novák, *J. Lumin.* **2009**, *129*, 1606 – 1609.
[8] P. Gawryszewska, J. Sokolnicki, J. Legendziewicz, *Coord. Chem. Rev.* **2005**, *249*, 2489 – 2509.
[9] K. Binnemans, *Chem. Rev.* **2009**, *109*, 4283 – 4374.

[10] B. G. Wybourne, *Spectroscopic Properties of Rare Earths*, Interscience Publishers, New York, **1965**.
[11] J. C. Krupa, *Inorg. Chim. Acta* **1987**, *139*, 223 – 241.
[12] V. S. Sastri, J. C. Bünzli, J. R. Perumareddi, V. R. Rao, G. V. S. Rayudu, *Modern aspects of rare earths and their complexes*, Elsevier, Amsterdam **2003**.
[13] N. Sabbatini, M. Guardigli, J. M. Lehn, *Coord. Chem. Rev.* **1993**, *123*, 201 – 228.
[14] E. R. Souaya, W. G. Hanna, E. H. Ismail, N. E. Milad, *Molecules* **2000**, *5*, 1121 – 1129.
[15] C. H. Ko, P. J. Chen, S. H. Chen, F. C. Chang, F. C. Lin, K. K. Chen, *Bioresour. Technol.* **2010**, *101*, 1528 – 1531.
[16] M. Latva, J. Kankare, *J. Coord. Chem.* **1998**, *43*, 121 – 142.
[17] M. A. Abubaker, K. Harrington, R. von Wandruszka, *Anal. Lett.* **1993**, *26*, 1681 – 1692.
[18] E. R. Souza, I. G. N. Silva, E. E. S. Teotonio, M. C. F. C. Felinto, H. F. Brito, *J. Lumin.* **2009**, *130*, 283 – 291.
[19] L. C. Yu, S. L. Liu, E. X. Liang, C. L. Wen, *J. Coord. Chem.* **2007**, *60*, 2097 – 2105.
[20] K. Nakamoto, *Infrared and Raman Spectra of Inorganic and Coordination Compounds*, Wiley, New York **1997**.
[21] R. K. Frost, F. C. Hagemeister, C. A. Arrington, D. Schleppenbach, T. Zwierl, K. D. Jordan, *J. Chem. Phys.* **1996**, *105*, 2605 – 2618.
[22] H. F. Brito, O. L. Malta, M. C. F. C. Felinto, E. E. S. Teotonio in *The Chemistry of Metal Enolates*, Part 1, (Ed.: J. Zabicky) John Wiley & Sons, Chichester, **2009**, chapter 3, pp. 131 – 184.
[23] N. Filipescu, W. F. Sager, F. A. Serafin, *J. Phys. Chem.* **1964**, *68*, 3324 – 3346.
[24] F. S. Richardson, *Chem. Rev.* **1982**, *82*, 541 – 552.
[25] D. F. Parra, A. Mucciolo, H. F. Brito, *J. Appl. Polym. Sci.* **2004**, *94*, 865 – 870.
[26] M. Latva, H. Takalo, V. M. Mukkala, C. Matachescu, J. C. Rodriguez-Ubis, J. Kankare, *J. Lumin.* **1997**, *75*, 149 – 169.
[27] S. Biju, M. L. P. Reddy, R. O. Freire, *Inorg. Chem. Commun.* **2007**, *10*, 393 – 396.
[28] I. G. N Silva, J. Kai, M. C. F. C. Felinto, H. F. Brito, *Opt. Mater.* **2013**, *35*, 978 – 982.
[29] G. F. de Sá, O. L. Malta, C. D. Donega, A. M. Simas, R. L. Longo, P. A. Santa-Cruz, E. F. Silva, *Coord. Chem. Rev.* **2000**, *196*, 165 – 195.
[30] D. B. Ambili Raj, S. Biju, M. L. P. Reddy, *Inorg. Chem.* **2008**, *47*, 8091 – 8100.
[31] E. E. S. Teotonio, G. M. Fett, H. F. Brito, W. M. Faustino, G. F. de Sa, M. C. F. C. Felinto, R. H. A. Santos, *J. Lumin.* **2008**, *128*, 190 – 198.
[32] W. T. Carnall, H. Crosswhite, H. M. Crosswhite, *Energy level structure and transition probabilities in the spectra of the trivalent lanthanides in* LaF_3, Rep. ANL-78-XX-95, Argonne National Laboratory, Argonne, IL (USA) **1978**.
[33] L. D. Carlos, Y. Messaddeq, H. F. Brito, R. A. S. Ferreira, V. de Zea Bermudez, S. J. L. Ribeiro, *Adv. Mater.* **2000**, *12*, 594 – 598.
[34] R. A. Sá Ferreira, S. S. Nobre, C. M. Granadeiro, H. I. S. Nogueira, L. D. Carlos, O. L. Malta, *J. Lumin.* **2006**, *121*, 561 – 567.
[35] P. A. Santa-Cruz, F. S. Teles, Software SPECTRA LUX (version 2.0 Beta), Ponto Quântico Nanodispositivos, RENAMI, **2003**.